

LORD: LOWER-DIMENSIONAL EMBEDDING OF LOG-SIGNATURE IN NEURAL ROUGH DIFFERENTIAL EQUATIONS

Jaehoon Lee, Jinsung Jeon, Sheoyon Jhin, Jihyeon Hyeong, Jayoung Kim,
Minju Jo, Seungji Kook, and Noseong Park

Yonsei University

Seoul, South Korea

{jaehoonlee, jjsjjs0902, sheoyonj, jiji.hyeong, jayoung.kim,
alf1sowl12, 2021321393, noseong}@yonsei.ac.kr

ABSTRACT

The problem of processing very long time-series data (e.g., a length of more than 10,000) is a long-standing research problem in machine learning. Recently, one breakthrough, called neural rough differential equations (NRDEs), has been proposed and has shown that it is able to process such data. Their main concept is to use the log-signature transform, which is known to be more efficient than the Fourier transform for irregular long time-series, to convert a very long time-series sample into a relatively shorter series of feature vectors. However, the log-signature transform causes non-trivial spatial overheads. To this end, we present the method of **LO**wer**R**-**D**imensional embedding of log-signature (LORD), where we define an NRDE-based autoencoder to implant the higher-depth log-signature knowledge into the lower-depth log-signature. We show that the encoder successfully combines the higher-depth and the lower-depth log-signature knowledge, which greatly stabilizes the training process and increases the model accuracy. In our experiments with benchmark datasets, the improvement ratio by our method is up to 75% in terms of various classification and forecasting evaluation metrics.

1 INTRODUCTION

Time-series data occurs frequently in real-world applications, e.g., stock price forecasting (Ariyo et al., 2014; Siami-Namini et al., 2018; Jhin et al., 2021), traffic forecasting (Reinsel, 2003; Fu, 2011; Bai et al., 2020; Fang et al., 2021), weather forecasting (Shi et al., 2015; Seo et al., 2018; Brouwer et al., 2019; Ren et al., 2021), and so on. However, it is known that very long time-series data (e.g., a time-series length of more than 10,000) is not straightforward to process with deep learning despite various techniques ranging from recurrent neural networks (RNNs) to neural ordinary/controlled differential equations (NODEs and NCDEs). RNNs are known to be unstable when training with such very long sequences and the maximum length that can be processed by NODEs and NCDEs is more or less the same as that by RNNs (Morrill et al., 2021; Aicher et al., 2020; Trinh et al., 2018; Stoller et al., 2019; Bai et al., 2018). However, one breakthrough has been recently proposed, namely neural rough differential equations (NRDEs).

NRDEs are based on the rough path theory which was established to make sense of the controlled differential equation:

$$dz(t) = f(z(t))dX(t), \quad (1)$$

where X is a continuous control path, and $\mathbf{z}(t)$ is a hidden vector at time t . A prevalent example of X is a (semimartingale) Wiener process, in which case the equation reduces to a stochastic differential equation. In this sense, the rough path theory extends stochastic differential equations beyond the semimartingale environments (Lyons et al., 2004).

One key concept in the rough path theory is the *log-signature* of a path. It had been proved that the log-signature of a path with bounded variations is unique under mild conditions (Lyons & Xu,

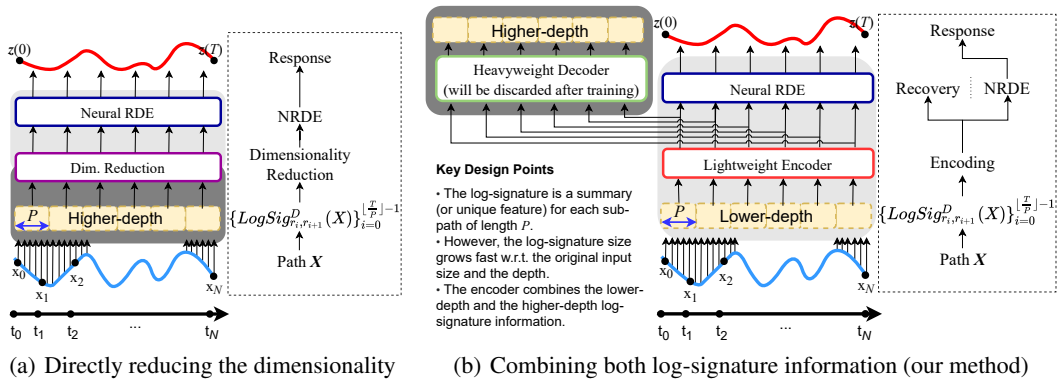


Figure 1: Two possible approaches to reduce the dimensionality of the higher-depth log-signature. The dark gray means a processing in a higher-dimensional space and the light gray means that in a lower-dimensional space. Our embedding method in (b) is better than the baseline in (a) in that i) the higher-dimensional processing is deferred to the decoder which will be discarded after pre-training the autoencoder, and ii) our method does not involve any higher-dimensional processing during the main training and inference processes. We pre-train the autoencoder and in the main training step, we discard the decoder, fix the encoder, and train only the main NRDE for a downstream task (cf. Table 1). In this way, we can exclude the higher-dimensional processing as early as possible.

2018; Geng, 2017) and most time-series data that happens in the field of deep learning has bounded variations. Therefore, one can interpret that the log-signature is a unique feature of the path.

Given a N -length time-series sample $\{\mathbf{x}_i\}_{i=0}^N$ annotated with its observation time-points $\{t_i\}_{i=0}^N$, where $t_0 = 0$, $t_N = T$, and $t_i < t_{i+1}$, NRDEs construct a continuous path $X(t)$, where $t \in [0, T]$, with an interpolation algorithm, where $X(t_i) = (\mathbf{x}_i, t_i)$ for $t_i \in \{t_i\}_{i=0}^N$. In other words, the path has the same value as the observation (\mathbf{x}_i, t_i) , when t_i is one of the observation time-points and otherwise, interpolated values. As shown in Fig. 1, a log-signature (each dotted yellow box in the figure) is calculated every P -length sub-path, and another time-series of log-signatures, denoted $\{LogSig_{r_i, r_{i+1}}^D(X)\}_{i=0}^{\lfloor \frac{T}{P} \rfloor - 1}$, is created. The log-signature calculation has one important hyperparameter D called *depth* — the higher the depth is, the more accurately represented each sub-path is (cf. Eq. 4). For instance, the best accuracy score is 0.81 for $D = 3$ vs. 0.78 for $D = 2$ in EigenWorms. The sub-path length P and the depth D decides the number and the dimensionality of log-signatures, respectively.

However, one downside is $\dim(LogSig_{r_i, r_{i+1}}^D(X)) > \dim(X)$, where $\dim(X)$ means the dimensionality (or the number of channels) of X . As a matter of fact, $\dim(LogSig_{r_i, r_{i+1}}^D(X))$ grows rapidly w.r.t. $\dim(X)$ (Morrill et al., 2021). Since the dimensionality of the input data is, given a dataset, fixed, we need to decrease D to reduce overheads. In general, NRDEs require more parameters to process higher-dimensional log-signatures (as shown in Table 4 where the original NRDE design always requires more parameters for $D = 3$ in comparison with $D = 2$).

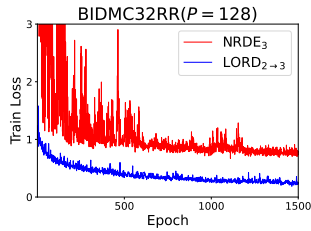


Figure 2: The loss curve of LORD is stable. Other figures are in Appendix F.

To this end, we propose to embed the higher-depth signatures onto a lower-dimensional space to i) decrease the complexity of the main NRDE (the solid blue box in Fig. 1), and ii) increase the easiness of training (cf. Fig. 2) and as a result, its model accuracy as well. Fig. 1 shows two possible approaches where we directly reduce the dimensionality of the higher-depth log-signature in Fig. 1 (a) or we adopt the autoencoder architecture to combine both the higher-depth and the lower-depth signatures in Fig. 1 (b) — the first approach in Fig. 1 (a) is a baseline model, and our proposed model is the second approach in Fig. 1 (b). Autoencoders are frequently used for (unsupervised) dimensionality reduction although there also exist other approaches. Since the higher-depth log-signature should be reconstructed from the embedded vector, one can consider that

the higher-depth log-signature is indirectly embedded into the vector. Moreover, the decoder is discarded after its pre-training so our method does not involve any high-cost computation with the higher-depth log-signature in the main training and inference steps as clarified in Table 1.

Table 1: Two phase training in our method

	Pre-training	Main training
Decoder	Training	Discarded
Encoder	Training	Fixed
Main NRDE	Not Applicable	Training

Our proposed method, **LOWeR-Dimensional** embedding of log-signature (LORD), adopts an NRDE-based autoencoder to combine the higher-depth and the lower-depth log-signature knowledge, and utilizes the embedded knowledge by the encoder for a downstream machine learning task as shown in Fig. 1 (b). The encoder embeds the lower-depth log-signature from the continuous

path X , and the decoder reconstructs the higher-depth log-signature. This specific design is where our key idea lies in. The encoded lower-depth log-signature will contain both the lower-depth and the higher-depth log-signature knowledge because i) it is an encoding of the lower-depth log-signature and ii) the decoder should recover the higher-depth log-signature from it. After pre-training the autoencoder, we discard the decoder to exclude the higher-dimensional processing as early as possible from our framework. After that, we fix the encoder and train only the main NRDE.

We conduct experiments with six very long time-series benchmark datasets and five baselines including NODE, NCDE, and NRDE-based models. RNN-based models cannot process the very long time-series datasets and we exclude them. Our proposed method significantly outperforms all existing baselines. Our contributions can be summarized as follows:

1. We design an NRDE-based *continuous* autoencoder to combine the higher-depth and the lower-depth log-signature information. Since the decoder is discarded after being trained, we adopt the asymmetric architecture that the encoder is lightweight and the decoder is heavyweight in terms of the number of parameters.
2. Our proposed method outperforms all baselines by large margins (up to 75% for various evaluation metrics, e.g., R^2) in standard benchmark datasets with much smaller model sizes in comparison with the original NRDE design.

Our code is available in <https://github.com/leejaehoon2016/LORD>.

2 RELATED WORK AND PRELIMINARIES

NODEs NODEs (Chen et al., 2018) use the following equation:

$$\mathbf{z}(T) = \mathbf{z}(0) + \int_0^T f(\mathbf{z}(t), t; \theta_f) dt, \quad (2)$$

which means $\mathbf{z}(T)$ is solely defined by the initial value $\mathbf{z}(0)$ — the entire evolving path from $\mathbf{z}(0)$ to $\mathbf{z}(T)$ is defined by the initial value in ODEs. NODEs are not considered as a continuous analogue to RNNs but to residual networks (Chen et al., 2018).

NCDEs Let $\{\mathbf{x}_i\}_{i=0}^N$ be an N -length time-series sample and $\{t_i\}_{i=0}^N$ be its observation time-points. NCDEs are different from NODEs in that they use the following equation:

$$\mathbf{z}(T) = \mathbf{z}(0) + \int_0^T f(\mathbf{z}(t); \theta_f) dX(t) = \mathbf{z}(0) + \int_0^T f(\mathbf{z}(t); \theta_f) \frac{dX(t)}{dt} dt, \quad (3)$$

where $X(t)$ is a continuous interpolated path from $\{\mathbf{x}_i, t_i\}_{i=0}^N$, where $t_N = T$. In this regards, NCDEs can also be considered as a continuous analogue to RNNs. The adjoint sensitivity method can be used to decrease the space complexity of gradient calculation instead of backpropagation (Kidger et al., 2020).

However, NCDEs has an inherent disadvantage that they are weak at processing very long time-series samples, because NCDEs directly process the very long time-series samples.

Signature Transform Let $[r_i, r_{i+1}]$ be a time duration, where $r_i < r_{i+1}$. The signature of the time-series sample is defined as follows:

$$S_{r_i, r_{i+1}}^{i_1, \dots, i_k}(X) = \int_{r_i < t_1 < \dots < t_k < r_{i+1}} \prod_{j=1}^k \frac{dX^{i_j}}{dt}(t_j) dt_j,$$

$$Sig_{r_i, r_{i+1}}^D(X) = \left(\{S_{r_i, r_{i+1}}^i(X)\}_{i=1}^{\dim(X)}, \{S_{r_i, r_{i+1}}^{i,j}(X)\}_{i,j=1}^{\dim(X)}, \dots, \{S_{r_i, r_{i+1}}^{i_1, \dots, i_D}(X)\}_{i_1, \dots, i_D=1}^{\dim(X)} \right), \quad (4)$$

However, the signature has redundancy, e.g., $S_{a,b}^{1,2}(X) + S_{a,b}^{2,1}(X) = S_{a,b}^1(X)S_{a,b}^2(X)$ where we can know a value if knowing three others. The log-signature $LogSig_{r_i, r_{i+1}}^D(X)$ is then created after dropping the redundancy from the signature. In this work, we use this log-signature definition in default to design our method. By creating a log-signature for every P -length sub-path, the entire sequence length can be reduced — moreover, the log-signature is a unique feature of the sub-path (Lyons & Xu, 2018; Geng, 2017). For complexity reasons, we typically use the log-signature of depth $D \leq 3$ (Morrill et al., 2021).

NRDEs Owing to the log-signature transform of time-series, NRDEs (Morrill et al., 2021) are defined as follows:

$$g(X, t) = \frac{LogSig_{r_i, r_{i+1}}^D(X)}{r_{i+1} - r_i} \text{ for } t \in [r_i, r_{i+1}),$$

$$\mathbf{z}(T) = \mathbf{z}(0) + \int_0^T f(\mathbf{z}(t); \theta_f) g(X, t) dt, \quad (5)$$

where $LogSig_{r_i, r_{i+1}}^D(X)$ means the log-signature created from the path X within the interval $[r_i, r_{i+1})$. $\frac{LogSig_{r_i, r_{i+1}}^D(X)}{r_{i+1} - r_i}$ is a piecewise approximation of the time-derivative of the log-signature in the short interval $[r_i, r_{i+1})$. D means the depth of the log-signature. Once we define the sub-path length P , the intervals $\{[r_i, r_{i+1})\}_{i=0}^{\lfloor \frac{T}{P} \rfloor - 1}$ are decided, i.e., $P = r_{i+1} - r_i$ for all i . Then, the time-series of $LogSig_{r_i, r_{i+1}}^D(X)$ constitutes $\{LogSig_{r_i, r_{i+1}}^D(X)\}_{i=0}^{\lfloor \frac{T}{P} \rfloor - 1}$ in our notation.

NRDEs use Eq. 5 to derive $\mathbf{z}(T)$ from $\mathbf{z}(0)$, which can be considered as a continuous analogue to RNNs since it continuously reads the time-derivative of the log-signature. Therefore, $\mathbf{z}(T)$ is defined by the initial value $\mathbf{z}(0)$ and the sequence of the time-derivative of the log-signature. We can also use the adjoint sensitivity method to train NRDEs.

Long Sequence Time-series Input (LSTI) The problem of processing very long time-series data is a long standing research problem. There are three ways to solve the LSTI problem. First, it reduces the sequence through truncating/summarizing/sampling from a very long input sequence. However, this method may lose information affecting the prediction accuracy. The second is to give the gradient transformation. As the sequence becomes longer, the gradient vanishing problem occurs. Therefore, in (Aicher et al., 2020), the model is trained using only the gradient of the last step. It also solves the problem using auxiliary losses (Trinh et al., 2018). Finally, CNNs (Stoller et al., 2019; Bai et al., 2018) were used to solve the LSTI problem. The convolutional filter captures long term dependencies, but the receptive fields increase exponentially, breaking the sequence.

3 PROPOSED METHOD

We describe our proposed method, LORD-NRDE. We first clarify the motivation of our work and then describe our proposed model design.

Motivation It is known that NRDEs are a generalization of NCDEs (Morrill et al., 2021, Section 3.2). However, one problem in utilizing NRDEs in real-world environments is that $\dim(LogSig_{r_i, r_{i+1}}^D(X))$ is a rapidly growing function of $\dim(X)$ (Morrill et al., 2021, Section A).

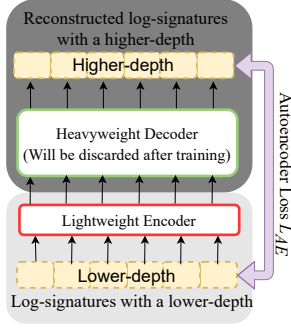


Figure 3: The proposed NRDE-based autoencoder

Algorithm 1: How to train LORD-NRDE

Input: Training data D_{train} , Validating data D_{val} , Maximum iteration numbers max_iter_{AE} and max_iter_{TASK}

- 1 Initialize the parameters of the encoder (i.e., $\theta_f, \theta_{\phi_e}$), the decoder (i.e., $\theta_o, \theta_{\phi_s}$), and the main NRDE (i.e., $\theta_g, \theta_{\phi_z}, \theta_{\phi_{output}}$);
- /* Pre-training of the autoencoder */
- 2 **for** max_iter_{AE} iterations **do**
- 3 | Train the encoder and the decoder using L_{AE} ;
- /* Main-training of LORD-NRDE */
- 4 **for** max_iter_{TASK} iterations **do**
- 5 | Train the main NRDE using L_{TASK} ;
- 6 | Validate the best main NRDE parameters with D_{val} ;
- 7 **return** the encoder and the main NRDE parameters;

This rapid blow-up of dimensionality causes two problems : i) it hinders us from applying NRDEs to high-dimensional time-series data, and ii) it makes the training process complicated since the hidden representation of the large input should be made for a downstream task. Therefore, we propose to embed the log-signature onto a lower dimensional space so that the training process becomes more tractable and enhance the applicability of NRDEs to high-dimensional data. After the embedding, in other words, the dimensionality of embedded vector is typically smaller than that of the log-signature with depth D_2 in our setting but it has knowledge of the log-signature with depth $D_2 > D_1$.

Overall Architecture We describe our proposed method, LORD-NRDE, which consists of three NRDEs: i) an encoder NRDE, ii) a decoder NRDE and iii) a main NRDE to derive $\mathbf{z}(T)$ from $\mathbf{z}(0)$. The role of each NRDE is as follows:

1. The encoder NRDE *continuously* embeds the log-signature with depth D_1 onto another space. We use $\mathbf{e}(t)$ to denote the vector embedded from the log-signature at time t .
2. The decoder NRDE reconstructs the log-signature with depth $D_2 > D_1$ from $\mathbf{e}(t)$.
3. The main NRDE reads $\mathbf{e}(t)$ to evolve $\mathbf{z}(t)$ and derive $\mathbf{z}(T)$. There is an output layer which reads $\mathbf{z}(T)$ and makes inference.

We note that $\dim(\text{LogSig}_{r_i, r_{i+1}}^{D_2}(X)) > \dim(\mathbf{e}(t))$, where $t \in [0, T]$. We require that the encoder produces embedding vectors that contain both the log-signature knowledge with D_1 and D_2 depth.

LORD-NRDE To this end, we propose the following method:

$$\mathbf{z}(T) = \mathbf{z}(0) + \int_0^T g(\mathbf{z}(t); \theta_g) \frac{d\mathbf{e}(t)}{dt} dt, \quad (6)$$

$$\mathbf{e}(T) = \mathbf{e}(0) + \int_0^T f(\mathbf{e}(t); \theta_f) \frac{\text{LogSig}_{r_i, r_{i+1}}^{D_1}(X)}{r_{i+1} - r_i} dt, \text{ for } t \in [r_i, r_{i+1}), \quad (7)$$

$$\mathbf{s}(T) = \mathbf{s}(0) + \int_0^T o(\mathbf{s}(t); \theta_o) \frac{d\mathbf{e}(t)}{dt} dt, \quad (8)$$

where $\dim(\mathbf{e}(t)) < \dim(\mathbf{s}(t)) = \dim(\text{LogSig}_{r_i, r_{i+1}}^{D_2}(X))$, where $t \in [r_i, r_{i+1})$, with $D_2 > D_1$.

The term $d\mathbf{e}(t)$ can be considered as an embedding of the log-signature with depth D_1 at time t , and $\mathbf{e}(t)$ as an embedding of $X(t)$ constructed by the log-signature with depth D_1 . Similarly, $d\mathbf{s}(t)$ is a reconstructed log-signature with depth D_2 from the embedding, and $\mathbf{s}(t)$ as $X(t)$ reconstructed by the log-signature with depth D_2 . Since $\mathbf{e}(0)$ and $\mathbf{s}(0)$ mean the initial values, we set $\phi_e(X(0); \theta_{\phi_e})$, $\phi_s(\mathbf{e}(0); \theta_{\phi_s})$, where ϕ means a transformation function.

Therefore, $\mathbf{e}(t)$ and $\mathbf{s}(t)$ constitute an autoencoder based on NDREs as shown in Fig. 3. In our design, we use the asymmetrical setting for them, where the encoder RDE is lightweight and the decoder RDE is heavyweight in terms of the number of parameters, considering the applicability of

our design to real-world environments. Since the decoder NRDE is discarded after its pre-training, the heavyweight setting causes no problems afterwards — our method requires more resources for the pre-training process though.

There are three functions g , f , and o in Eqs. 6 to 8 and their definitions are as follows:

$$g(\mathbf{z}(t); \theta_g) = \text{FC}_{out_g, N_g+1}(\psi(\text{FC}_{h_g, N_g}(\dots \eta(\text{FC}_{h_g, 1}(\mathbf{z}(t)) \dots))), \quad (9)$$

$$f(\mathbf{e}(t); \theta_f) = \text{FC}_{out_f, N_f+1}(\psi(\text{FC}_{h_f, N_f}(\dots \eta(\text{FC}_{h_f, 1}(\mathbf{e}(t)) \dots))), \quad (10)$$

$$o(\mathbf{s}(t); \theta_o) = \text{FC}_{out_o, N_o+1}(\psi(\text{FC}_{h_o, N_o}(\dots \eta(\text{FC}_{h_o, 1}(\mathbf{s}(t)) \dots))), \quad (11)$$

where FC_h is a fully-connected (FC) layer whose output size is h . N_g, N_f, N_o means the number of FC layers. ψ and η are the hyperbolic tangent and rectified linear unit activations, respectively.

Training Method To train the NRDE-based autoencoder, we use the following loss:

$$L_{recon} = \frac{\sum_{i=0}^M \|(\mathbf{s}(r_{i+1}) - \mathbf{s}(r_i)) - \text{LogSig}_{r_i, r_{i+1}}^{D_2}(X)\|_2^2}{M}, \quad (12)$$

$$L_{AE} = L_{recon} + c_{AE}(\|\theta_f\|_2^2 + \|\theta_o\|_2^2 + \|\theta_{\phi_e}\|_2^2 + \|\theta_{\phi_s}\|_2^2) + c_e\|\mathbf{e}\|_2^2, \quad (13)$$

where $M = \lfloor \frac{T}{P} \rfloor - 1$, and c_{AE} is a coefficient of the L_2 regularization terms. c_e also regularizes the scale of the learned embedding. In addition to L_{AE} , we also have a task loss L_{TASK} which is the standard cross-entropy (CE) loss or the mean squared loss (MSE) loss. From $\mathbf{z}(T)$, we have an output layer, which is typically a fully-connected layer with an appropriate final activation function such as softmax, to produce a prediction \hat{y} . $\theta_{\phi_{\text{output}}}$ denotes the parameters of the output layer. Using the ground-truth information y , we define the task loss L_{TASK} . Therefore, the final loss can be written as follows:

$$L_{TASK} = CE(y, \hat{y}) + c_{TASK}(\|\theta_g\|_2^2 + \|\theta_{\phi_z}\|_2^2 + \|\theta_{\phi_{\text{output}}}\|_2^2), \quad (14)$$

where c_{TASK} is a coefficient of the L_2 regularization terms, and $CE(y, \hat{y})$ means a cross-entropy loss — we assume classification but it can be accordingly changed for other tasks.

To implement, we define the following augmented ODE:

$$\frac{d}{dt} \begin{bmatrix} \mathbf{z}(t) \\ \mathbf{e}(t) \\ \mathbf{s}(t) \end{bmatrix} = \begin{bmatrix} g(\mathbf{z}(t); \theta_g) f(\mathbf{e}(t); \theta_f) \frac{\text{LogSig}_{r_i, r_{i+1}}^{D_1}(X)}{r_{i+1} - r_i} \\ f(\mathbf{e}(t); \theta_f) \frac{\text{LogSig}_{r_i, r_{i+1}}^{D_1}(X)}{r_{i+1} - r_i} \\ o(\mathbf{s}(t); \theta_o) f(\mathbf{e}(t); \theta_f) \frac{\text{LogSig}_{r_i, r_{i+1}}^{D_1}(X)}{r_{i+1} - r_i} \end{bmatrix}, \text{ for } t \in [r_i, r_{i+1}), \quad (15)$$

where we replace $\frac{d\mathbf{e}(t)}{dt}$ with $f(\mathbf{e}(t); \theta_f) \frac{\text{LogSig}_{r_i, r_{i+1}}^{D_1}(X)}{r_{i+1} - r_i}$ (as defined in Eq. 7), and the initial values are defined as follows:

$$\begin{bmatrix} \mathbf{z}(0) \\ \mathbf{e}(0) \\ \mathbf{s}(0) \end{bmatrix} = \begin{bmatrix} \phi_z(X(0)); \theta_{\phi_z} \\ \phi_e(X(0)); \theta_{\phi_e} \\ \phi_s(\mathbf{e}(0)); \theta_{\phi_s} \end{bmatrix}, \quad (16)$$

where ϕ_z and ϕ_e are transformation functions to produce the initial values from the initial observation $X(0)$, and ϕ_s is a transformation function to produce the initial reconstructed value from the initial embedded vector $\mathbf{e}(0)$. We use a fully-connected layer for each of them.

Alg. 1 shows the training algorithm. In Line 3, we pre-train the autoencoder for $max.iter_{AE}$ iterations. After discarding the decoder and fixing the encoder, we then train the main NRDE in Line 5 for $max.iter_{TASK}$ iterations. Using D_{val} , we validate and choose the best parameters.

4 EXPERIMENTAL EVALUATIONS

We describe our experimental environments and results. The mean and variance of 5 different seeds are reported for model evaluation. We refer to Appendix A for reproducibility.

4.1 EXPERIMENTAL ENVIRONMENTS

Datasets We use six real-word dataset which all contain very long time-series samples. There are 3 classification datasets in the University of East Anglia (UEA) repository (Bagnall A.): EigenWorms, CounterMovementJump, and SelfRegulationSCP2, and 3 forecasting datasets in Beth Israel Deaconess Medical Centre (BIDMC) which come from the TSR archive (Bagnall A.): BIDMCHR, BIDMCRR, BIDMCSpO2. We refer to Appendix B for detail of datasets.

Baselines There are three types of baselines in our Experiments, ranging from NODE to NCDE and NRDE-based baseline models. ODE-RNN is one of the state-of-the-art NODE models in processing time-series. Following the suggestion in (Morrill et al., 2021), we merge P observations into one merged observation and feed it into ODE-RNN, in which case ODE-RNN is able to process much longer time-series. The dimensionality of the merged observation is P times larger than that of the original observation or equivalently, the length of the merged time-series is P times shorter than that of the original one. NCDE is the original NCDE design in (Kidger et al., 2020). Attentive NCDE (ANCDE) is an extension of NCDE by adding an attention mechanism into it, which significantly outperforms NCDE (Jhin et al., 2021). For the NRDE-type baselines, we consider i) the original NRDE design (Morrill et al., 2021), and ii) the one in Fig. 1 (a) which directly embeds the higher-depth log-signature into a lower-dimensional space, each of which is called NRDE and DE-NRDE, respectively. For those NRDE-based models, we clarify its one important hyperparameter, *depth*, as part of its name, e.g., NRDE₂ means NRDE with $D = 2$. One important point is that NRDE is a generalization of NCDE. Therefore, NRDE₁ is theoretically identical to NCDE, if using the linear interpolation method, and for this reason, we set $D > 1$ for NRDE.

Hyperparameters When using NRDEs, there is one crucial hyperparameter, the log-signature depth D . We use two depth settings which were used in (Morrill et al., 2021). For our LORD-NRDE, there are two depths, D_1 and D_2 , where $D_1 < D_2$. LORD _{$D_1 \rightarrow D_2$} means that LORD-NRDE’s decoder recovers the D_2 -depth log-signature from the D_1 -depth log-signature. The number of layers in the encoder, decoder and main NRDE, N_g , N_f , and N_o of Eqs. 9 to 11, are in $\{2, 3\}$. The hidden sizes, h_g , h_f , and h_o of Eqs. 9 to 11, are in $\{32, 64, 128, 192\}$. The coefficients of the L_2 regularizers in Eqs. 13 and 14 are in $\{1 \times 10^{-5}, 1 \times 10^{-6}\}$. The coefficient of the embedding regularizer, c_e in Eq. 13 is in $\{0, 1, 10\}$. The max iteration numbers, $max.iter_{AE}$ and $max.iter_{TASK}$ in Alg. 1, are in $\{400, 500, 1000, 1500, 2000\}$. The learning rate of the pre-training and main-training is 1×10^{-3} . We also set $\dim(\mathbf{e}(t)) = \dim(\text{LogSig}_{r_i, r_{i+1}}^{D_1}(X))$, where $t \in [r_i, r_{i+1})$.

We also conduct experiments by setting the sub-path length P to 4, 8, 32, 64, 128, 256, or 512 observations. In other words, we create one log-signature for every P input observation for NCDE and NRDE-based models. For ODE-RNN, as described earlier, we simply concatenate P observations into one observation. The final time T is large in our experiments, e.g., $T > 10,000$, and the number of log-signatures is $\lfloor \frac{T}{P} \rfloor$. We test both the adjoint sensitivity method and the backpropagation through the solver.

Evaluation Methods We reuse the very long time-series classification and forecasting evaluation methods of (Morrill et al., 2021) and extend the methods by adding more datasets and more evaluation metrics. We use accuracy, macro F1, and ROCAUC for binary classification; accuracy, macro/weighted F1, and ROCAUC for multi-class classification; and R^2 , explained variance, mean squared error (MSE), and mean absolute error (MAE) for forecasting — we list the complete results in Appendix D after introducing key results in the main manuscript. We also show the number of parameters for each model — for our LORD, we exclude the parameter numbers of the decoder since it is discarded after the pre-training. We train and test each model 5 times with different seeds. If the mean of score is the same, the smaller standard deviation is better.

4.2 EXPERIMENTAL RESULTS

Summary of Experimental Results Since our main result tables have many items, we quickly summarize their highlights in Tables 2 and 3. To calculate the improvement in evaluation metrics, we use the ratio of improvement over NRDE₂ for each metric averaged over all the sub-path lengths and all datasets, e.g., we calculate $\frac{\text{LORD's ROCAUC} - \text{NRDE}_2\text{'s ROCAUC}}{\text{NRDE}_2\text{'s ROCAUC}}$ and $\frac{\text{NRDE}_2\text{'s MSE} - \text{LORD's MSE}}{\text{NRDE}_2\text{'s MSE}}$ for all classification cases and average them. The ratio of the number of parameters is calculated similarly.

Table 2: Highlights in Classification

Method	Acc.	Mac.FI	ROCAUC	#Params
ODE-RNN	-9%	-19%	-11%	-20%
NCDE	-4%	-8%	-5%	-64%
ANCDE	0%	0%	0%	15%
NRDE ₂	0%	0%	0%	0%
NRDE ₃	2%	4%	2%	537%
DE-NRDE ₂	-4%	-7%	-3%	-48%
DE-NRDE ₃	-2%	-2%	0%	177%
LORD _{1→2}	16%	23%	11%	-55%
LORD _{1→3}	15%	20%	10%	-46%
LORD _{2→3}	8%	9%	4%	17%

Table 3: Highlights in Forecasting

Method	R ²	MSE	#Params
ODE-RNN	44%	41%	-36%
NCDE	-45%	-55%	-30%
ANCDE	-34%	-45%	-52%
NRDE ₂	0%	0%	0%
NRDE ₃	0%	-5%	82%
DE-NRDE ₂	39%	35%	-20%
DE-NRDE ₃	62%	59%	31%
LORD _{1→2}	53%	47%	-65%
LORD _{1→3}	51%	46%	-59%
LORD _{2→3}	75%	72%	-39%

Overall, LORD outperforms other baselines with smaller numbers of parameters. LORD_{D₁→D₂} has a larger model size, excluding its decoder, than NRDE_{D₁} whereas it has a much smaller model size than NRDE_{D₂}. However, the performance of LORD_{D₁→D₂} is similar to or better than that of NRDE_{D₂}, which proves the efficacy of our method. Using the encoder-decoder structure, the high complexity of processing log-signatures can be reduced and it makes our model smaller and more amenable to train.

In many cases for LORD, the adjoint method and the backpropagation method are comparable in terms of model accuracy. Interestingly, we found that the backpropagation through the Euler method is fast enough with a neglectable sacrifice of accuracy for several cases.

Detailed Experimental Results Table 4 show detailed results for some selected evaluation metrics — full tables with all metrics are in Appendix D. One point is that many best outcomes are made with moderate P settings. For EigenWorms, ODE-RNN can’t achieve good scores for all P settings. Our proposed model, LORD, achieves the best scores. In particular, LORD_{1→3} with $P = 32$ has a much smaller number of parameters, compared with other baselines that have similar performance. LORD_{2→3} also significantly outperforms NRDE₃ for both accuracy and mode size. For CounterMovementJump and SelfRegulationSCP2, ODE-RNN is better than other NRDE and NCDE-based baselines. However, LORD marks the best scores in all cases.

In all BIDMC experiments, LORD shows outstanding performance. LORD_{2→3} shows the best performance in almost all cases. Compared with NCDE and NRDE, DE-NRDE has 40 ~ 60% improvements and LORD has 50 ~ 70% improvements. However, LORD’s model size is reduced by 60% whereas DE-NRDE’s model size is reduced by 20%. Therefore, our proposed method is a better embedding method for log-signatures. Unlike EigenWorms, the time-series length in this dataset is rather short. For that reason, ODE-RNN performs better. Overall, DE-NRDE₃ with $P = 128$ has the best performance, among the baseline models. This means that the training difficulty by the large log-signature size can be alleviated by the direct embedding. However, LORD outperforms DE-NRDE.

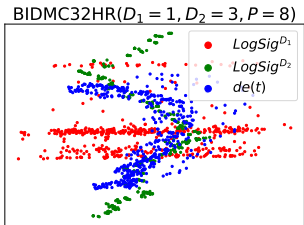


Figure 4: PCA-based visualization of log-signatures

Additional Results and Visualization Fig. 4 visually compares the three log-signatures and we note that the embedded signature of $de(t)$ has the characteristics of both $D_1 = 1$ and $D_2 = 3$. We refer to our supplementary material for other visualization, detailed results, sensitivity analyses, and reproducibility information.

5 LIMITATIONS AND CONCLUSIONS

The log-signature transform of NRDEs is suitable to irregular and long time-series. However, the log-signature transform requires larger memory footprints and to this end, we presented an autoencoder-based method to embed their higher-dimensional log-signature into a lower-dimensional space, called LORD. Our method is carefully devised to eradicate the higher-dimensional computation as early as right after the pre-training of the autoencoder. In the standard benchmark experiments of very long time-series, our proposed method significantly outperforms existing methods and shows relatively smaller model sizes in terms of the number of parameters. Nonetheless, it is still in its early phase to enhance NRDEs and there exist a couple of items to be studied further, e.g., processing long time-series with many channels.

6 ACKNOWLEDGEMENTS

Noseong Park is the corresponding author. This work was supported by the Yonsei University Research Fund of 2021, and the Institute of Information & Communications Technology Planning & Evaluation (IITP) grant funded by the Korean government (MSIT) (No. 2020-0-01361, Artificial Intelligence Graduate School Program (Yonsei University), and No. 2021-0-00155, Context and Activity Analysis-based Solution for Safe Childcare).

REFERENCES

- Christopher Aicher, Nicholas J Foti, and Emily B Fox. Adaptively truncating backpropagation through time to control gradient bias. In *Uncertainty in Artificial Intelligence*, pp. 799–808. PMLR, 2020.
- Adebiyi A. Ariyo, Adewumi O. Adewumi, and Charles K. Ayo. Stock price prediction using the arima model. 2014.
- Keogh E. Bagnall A. Uea classification/regression datasets. <http://www.timeseriesregression.org/>, <http://www.timeseriesclassification.com/>.
- Lei Bai, Lina Yao, Can Li, Xianzhi Wang, and Can Wang. Adaptive graph convolutional recurrent network for traffic forecasting. In H. Larochelle, M. Ranzato, R. Hadsell, M. F. Balcan, and H. Lin (eds.), *NeurIPS*, volume 33, pp. 17804–17815, 2020.
- Shaojie Bai, J Zico Kolter, and Vladlen Koltun. Convolutional sequence modeling revisited. 2018.
- Edward De Brouwer, Jaak Simm, Adam Arany, and Yves Moreau. Gru-ode-bayes: Continuous modeling of sporadically-observed time series. In *NeurIPS*, 2019.
- Ricky T. Q. Chen, Yulia Rubanova, Jesse Bettencourt, and David K Duvenaud. Neural ordinary differential equations. In *NeurIPS*. 2018.
- Zheng Fang, Qingqing Long, Guojie Song, and Kunqing Xie. Spatial-temporal graph ode networks for traffic flow forecasting. *arXiv preprint arXiv:2106.12931*, 2021.
- Tak-chung Fu. A review on time series data mining. *Engineering Applications of Artificial Intelligence*, 24(1):164–181, 2011.
- Xi Geng. Reconstruction for the signature of a rough path. *Proceedings of the London Mathematical Society*, 114(3):495–526, 2017.
- Sheo Yon Jhin, Heejoo Shin, Seoyoung Hong, Minju Jo, Solhee Park, and Noseong Park. Attentive neural controlled differential equations for time-series classification and forecasting. In *ICDM*, 2021.
- Patrick Kidger, James Morrill, James Foster, and Terry Lyons. Neural controlled differential equations for irregular time series. In *NeurIPS*, 2020.
- Terry Lyons and Weijun Xu. Inverting the signature of a path, 2018.
- Terry Lyons, M. Caruana, and T. Lévy. *Differential Equations Driven by Rough Paths*. Springer, 2004. École D’Eté de Probabilités de Saint-Flour XXXIV - 2004.
- James Morrill, Cristopher Salvi, Patrick Kidger, James Foster, and Terry Lyons. Neural rough differential equations for long time series. 2021.
- Gregory C Reinsel. *Elements of multivariate time series analysis*. Springer Science & Business Media, 2003.
- Xiaoli Ren, Xiaoyong Li, Kaijun Ren, Junqiang Song, Zichen Xu, Kefeng Deng, and Xiang Wang. Deep learning-based weather prediction: A survey. *Big Data Research*, 23, 2021.

- Sungyong Seo, Arash Mohegh, George Ban-Weiss, and Yan Liu. Automatically inferring data quality for spatiotemporal forecasting. In *International Conference on Learning Representations*, 2018.
- Xingjian Shi, Zhourong Chen, Hao Wang, Dit-Yan Yeung, Wai-Kin Wong, and Wang-chun Woo. Convolutional lstm network: A machine learning approach for precipitation nowcasting. *NeurIPS*, 28, 2015.
- Sima Siami-Namini, Neda Tavakoli, and Akbar Siami Namin. A comparison of arima and lstm in forecasting time series. 2018.
- Daniel Stoller, Mi Tian, Sebastian Ewert, and Simon Dixon. Seq-u-net: A one-dimensional causal u-net for efficient sequence modelling. *arXiv preprint arXiv:1911.06393*, 2019.
- Trieu Trinh, Andrew Dai, Thang Luong, and Quoc Le. Learning longer-term dependencies in rnns with auxiliary losses. In *International Conference on Machine Learning*, pp. 4965–4974. PMLR, 2018.

Table 5: The best hyperparameter in ODE-RNN

Data	P	Hidden Path Size
Counter-MovementJump	64	64
	128	256
	512	64
Self-RegulationSCP2	32	128
	64	64
	256	64

Table 6: The best hyperparameter in NCDE and NRDE

Data	P	Hidden Path Size			CDE Function's Hidden Size			#Hidden Layers		
		$D = 1$	2	3	1	2	3	1	2	3
Counter-MovementJump	64	64	64	128	128	128	128	3	2	3
	128	64	256	256	64	64	64	3	2	3
	512	128	64	256	64	64	256	3	2	3
Self-RegulationSCP2	32	64	64	128	64	128	128	2	2	2
	64	64	256	128	256	64	64	3	2	2
	256	256	256	64	128	64	256	3	2	3

Table 7: The best hyperparameter in ANCDE

Data	P	Hidden Path Size	#Hidden Layers	Attention Channel Size
EigenWorms	4	128	3	64
	32	128	3	64
	128	64	2	32
Counter-MovementJump	64	128	2	128
	128	256	3	128
	512	64	2	256
Self-RegulationSCP2	32	256	3	128
	64	64	2	128
	256	128	2	128
BIDMC32HR	8	128	2	64
	128	128	2	64
	512	128	2	64
BIDMC32RR	8	128	2	64
	128	128	2	64
	512	128	3	64
BIDMC32SpO2	8	128	2	64
	128	128	2	64
	512	128	2	64

Table 8: The best hyperparameter in DE-NRDE

Data	P	Compression Ratio			#Hidden Layers			Hidden Size		
		$D = 2$	3	3	2	3	2	3	2	3
EigenWorms	4	0.5	0.5	1	1	128	128	128	128	
	32	0.5	0.5	1	1	128	128	128	128	
	128	0.7	0.7	1	1	64	128	128	128	
Counter-MovementJump	64	0.3	0.3	1	2	128	128	64	128	
	128	0.3	0.5	2	2	128	64	128	64	
	512	0.7	0.3	1	1	64	128	128	64	
Self-RegulationSCP2	32	0.3	0.3	1	2	64	128	64	128	
	64	0.3	0.3	2	2	64	64	64	64	
	256	0.3	0.3	2	2	64	128	64	128	
BIDMC32HR	8	0.7	0.7	2	2	64	128	128	128	
	128	0.7	0.7	1	1	128	128	128	128	
	512	0.7	0.7	1	1	64	128	128	128	
BIDMC32RR	8	0.5	0.5	1	1	128	128	128	128	
	128	0.7	0.7	1	1	128	128	128	128	
	512	0.7	0.7	1	1	64	64	64	64	
BIDMC32SpO2	8	0.5	0.5	1	1	128	128	128	128	
	128	0.7	0.7	1	1	64	64	64	64	
	512	0.7	0.7	1	1	64	64	64	64	

A BEST HYPERPARAMETERS

Our software and hardware environments are as follows: UBUNTU 18.04 LTS, PYTHON 3.7.10, PYTORCH 1.8.1, CUDA 11.4, and NVIDIA Driver 470.42.01, i9 CPU, and NVIDIA RTX A6000.

A.1 BASELINE

There are 5 baselines in our experiments. Each model has its own hyperparameters. ODE-RNN method has a hyperparameter of hidden path size. NCDE and NRDE have also the same hyperparameter, and in addition, the size of hidden dimension and the number of hidden layers in their CDE and RDE functions. The Attentive NCDE (ANCDE) has all of those hyperparameters and in addition, the attention channel size. In DE-NRDE, there are addition hyperparameters related to embedding, which are the embedding compression ratio, the size of hidden dimension, and the number of hidden layers in the embedding layer.

In (Morrill et al., 2021), there are three models, ODE-RNN, NCDE and NRDE, and four datasets, EigenWorms, BIDMC32HR, BIDMC32RR, and BIDMC32SpO2. For these combinations, we set the hyperparameters as reported in (Morrill et al., 2021). In other cases, we find the best hyperparameters in the following range. All kinds of hidden size in ODE-RNN, NCDE, ANCDE, and NRDE are in $\{32, 64, 128, 256\}$. The number of hidden layers in those is in $\{2, 3\}$. In DE-NRDE, the embedding compression ratio, the hidden size, and the number of hidden layers in the embedding layer are in $\{0.3, 0.5, 0.7\}$, $\{64, 128\}$, and $\{1, 2\}$, respectively. Tables 5 to 8 show the best hyperparameters of the baselines.

A.2 LORD-NRDE

Table 9 shows the best hyperparameter configuration of our method in each dataset.

Table 9: The best hyperparameter in LORD

Method	Data	P	N_f	N_g	N_o	h_f	h_g	h_o	c_{AE}	c_{TASK}	c_e	$max.iter$	AE	$TASK$
LORD _{1→2}	EigenWorms	4	3	3	3	64	64	64	1×10^{-6}	1×10^{-6}	0	400	400	
		32	3	3	3	64	64	64	1×10^{-6}	1×10^{-6}	0	2000	400	
		128	3	2	3	64	64	64	1×10^{-6}	1×10^{-6}	0	2000	400	
	Counter-MovementJump	64	2	3	2	32	128	32	1×10^{-6}	1×10^{-6}	1	500	400	
		128	3	3	3	64	64	64	1×10^{-6}	1×10^{-6}	1	500	400	
		512	2	2	2	64	128	64	1×10^{-6}	1×10^{-6}	1	1500	400	
	Self-RegulationSCP2	32	3	3	3	32	32	32	1×10^{-6}	1×10^{-6}	1	1000	400	
		64	3	2	3	128	128	128	1×10^{-6}	1×10^{-6}	1	500	400	
		256	3	3	3	128	32	128	1×10^{-6}	1×10^{-6}	1	500	400	
	BIDMC32HR	8	3	3	3	64	64	64	1×10^{-5}	1×10^{-5}	0	400	2000	
		128	3	3	3	32	64	32	1×10^{-5}	1×10^{-5}	0	1000	500	
		512	3	3	3	32	64	32	1×10^{-5}	1×10^{-5}	0	1000	500	
	BIDMC32RR	8	3	3	3	64	64	64	1×10^{-5}	1×10^{-5}	0	400	2000	
		128	3	3	3	64	64	64	1×10^{-5}	1×10^{-5}	0	1000	500	
		512	3	3	3	64	64	64	1×10^{-5}	1×10^{-5}	0	1000	500	
	BIDMC32SpO2	8	3	3	3	64	64	64	1×10^{-5}	1×10^{-5}	0	400	2000	
		128	3	3	3	32	64	32	1×10^{-5}	1×10^{-5}	0	1000	500	
		512	3	3	3	64	64	64	1×10^{-5}	1×10^{-5}	0	1000	500	
	LORD _{1→3}	EigenWorms	4	3	2	3	64	64	64	1×10^{-6}	1×10^{-6}	0	400	400
			32	3	2	3	64	64	64	1×10^{-6}	1×10^{-6}	0	2000	400
			128	3	3	3	64	64	64	1×10^{-6}	1×10^{-6}	0	2000	400
		Counter-MovementJump	64	2	3	2	32	64	32	1×10^{-6}	1×10^{-6}	1	500	400
			128	3	3	3	128	128	128	1×10^{-6}	1×10^{-6}	1	500	400
			512	3	2	3	32	128	32	1×10^{-6}	1×10^{-6}	1	500	400
Self-RegulationSCP2		32	2	3	2	32	128	32	1×10^{-6}	1×10^{-6}	1	500	400	
		64	3	3	3	32	128	32	1×10^{-6}	1×10^{-6}	1	1500	400	
		256	3	3	3	128	128	128	1×10^{-6}	1×10^{-6}	1	1500	400	
BIDMC32HR		8	3	3	3	128	64	128	1×10^{-5}	1×10^{-5}	0	400	2000	
		128	3	3	3	32	64	32	1×10^{-5}	1×10^{-5}	0	1000	500	
		512	3	3	3	32	64	32	1×10^{-5}	1×10^{-5}	0	1000	500	
BIDMC32RR		8	3	3	3	64	64	64	1×10^{-5}	1×10^{-5}	0	400	2000	
		128	3	3	3	64	64	64	1×10^{-5}	1×10^{-5}	0	1000	500	
		512	3	3	3	64	64	64	1×10^{-5}	1×10^{-5}	0	1000	500	
BIDMC32SpO2		8	3	3	3	64	64	64	1×10^{-5}	1×10^{-5}	0	400	2000	
		128	3	3	3	64	64	64	1×10^{-5}	1×10^{-5}	0	1000	500	
		512	3	3	3	32	64	32	1×10^{-5}	1×10^{-5}	0	1000	500	
LORD _{2→3}		EigenWorms	4	3	3	3	64	64	64	1×10^{-6}	1×10^{-6}	0	400	400
			32	3	3	3	64	64	64	1×10^{-6}	1×10^{-6}	0	2000	400
			128	3	2	3	64	64	64	1×10^{-6}	1×10^{-6}	0	2000	400
		Counter-MovementJump	64	3	2	3	128	128	128	1×10^{-6}	1×10^{-6}	1	1500	400
			128	2	2	2	64	128	64	1×10^{-6}	1×10^{-6}	1	1000	400
			512	3	2	3	64	32	64	1×10^{-6}	1×10^{-6}	1	1000	400
	Self-RegulationSCP2	32	3	2	3	32	64	32	1×10^{-6}	1×10^{-6}	1	500	400	
		64	2	3	2	128	128	128	1×10^{-6}	1×10^{-6}	1	1000	400	
		256	2	3	2	32	128	32	1×10^{-6}	1×10^{-6}	1	500	400	
	BIDMC32HR	8	3	3	3	64	64	64	1×10^{-5}	1×10^{-5}	0	400	2000	
		128	3	3	3	32	64	32	1×10^{-5}	1×10^{-5}	0	1000	500	
		512	3	3	3	64	64	64	1×10^{-5}	1×10^{-5}	0	1000	500	
	BIDMC32RR	8	3	3	3	64	64	64	1×10^{-5}	1×10^{-5}	0	400	2000	
		128	3	3	3	64	192	64	1×10^{-5}	1×10^{-5}	0	1000	500	
		512	3	3	3	128	64	128	1×10^{-5}	1×10^{-5}	0	1000	500	
	BIDMC32SpO2	8	3	3	3	64	64	64	1×10^{-5}	1×10^{-5}	0	400	2000	
		128	3	3	3	64	64	64	1×10^{-5}	1×10^{-5}	0	1000	500	
		512	3	3	3	128	64	128	1×10^{-5}	1×10^{-5}	0	1000	500	

B DATASET

EigenWorms has a time-series length of 17,984 and a channel of 7 which contains the movement data of roundworms. The goal is to classify each worm among 5 worm types. CounterMovementJump has 4,250 length and 4 channels which means accelerations data of each 3D-axis. Using accelerations data, the type of jump is predicted among 3 types. The object of SelfRegulationSCP2 is to classify whether the subject moves the computer’s cursor up or down, using 8 channels of the EEG data. Its time-series length is 1,153.

For forecasting, three Beth Israel Deaconess Medical Centre (BIDMC) datasets are used. Using the PPG and ECG information, each task is to predict a person’s heart rate (HR), respiratory rate (RR), or oxygen saturation (SpO2), respectively. The time-series length is 4,000.

C VISUALIZATION

We show other PCA based visualizations of the log-signatures. Using PCA, we extract the distributions of the most important principle components of $\{LogSig_{r_i, r_{i+1}}^{D_1}(X)\}_{i=0}^{\lfloor \frac{T}{P} \rfloor - 1}$, $\{LogSig_{r_i, r_{i+1}}^{D_2}(X)\}_{i=0}^{\lfloor \frac{T}{P} \rfloor - 1}$, and $de(t)$. If two paths have similar distributions on those components, the information contained by the two paths is similar. In Fig. 5, the distribution of $de(t)$ is somewhere in between the distributions of $\{LogSig_{r_i, r_{i+1}}^{D_2}(X)\}_{i=0}^{\lfloor \frac{T}{P} \rfloor - 1}$ and $\{LogSig_{r_i, r_{i+1}}^{D_1}(X)\}_{i=0}^{\lfloor \frac{T}{P} \rfloor - 1}$. From the encoder-decoder learning, $de(t)$ can learn the information of $\{LogSig_{r_i, r_{i+1}}^{D_2}(X)\}_{i=0}^{\lfloor \frac{T}{P} \rfloor - 1}$.

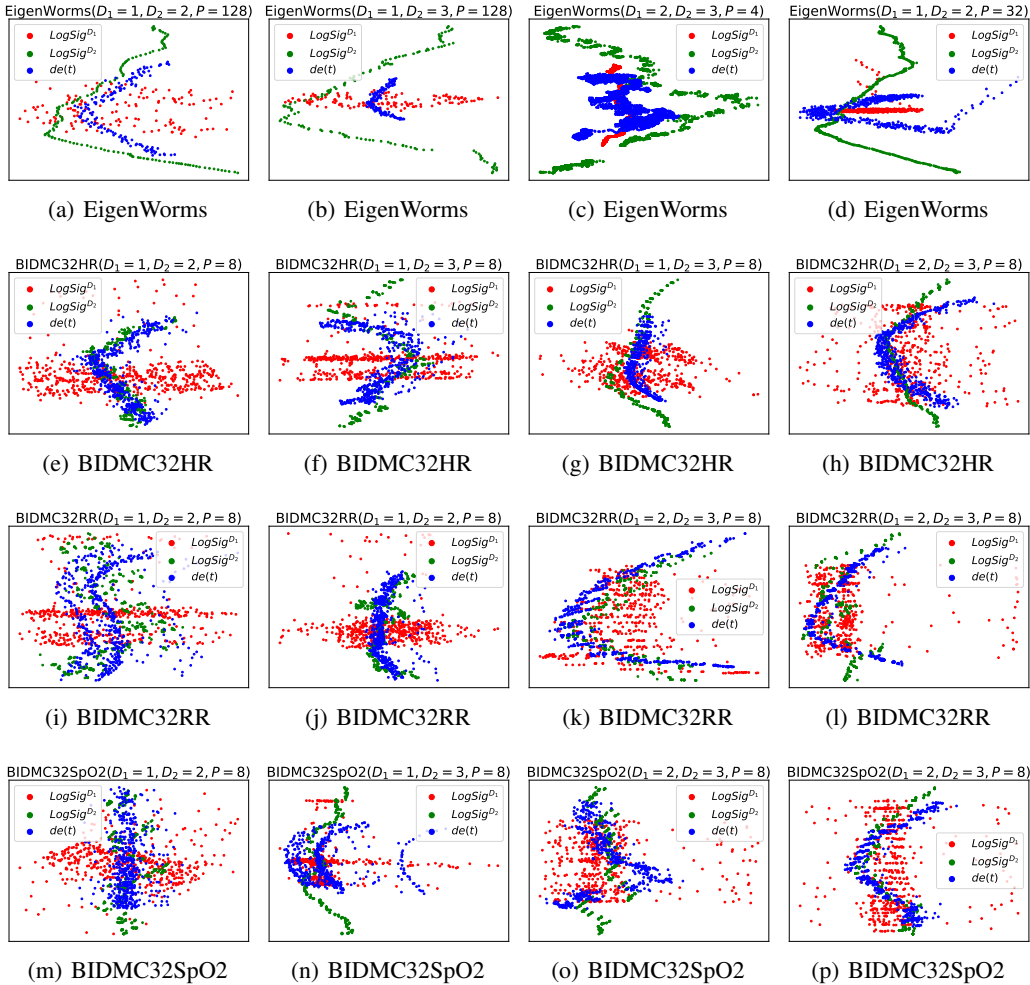


Figure 5: Visualization of $\{LogSig_{r_i, r_{i+1}}^{D_1}(X)\}_{i=0}^{\lfloor \frac{T}{P} \rfloor - 1}$, $\{LogSig_{r_i, r_{i+1}}^{D_2}(X)\}_{i=0}^{\lfloor \frac{T}{P} \rfloor - 1}$, and $de(t)$ in EigenWorms and BIDMC.

Table 10: EigenWorms

Method	P	Accuracy	Macro F1	Weighted F1	ROCAUC	#Params(D)	#Params(R)
ODE-RNN	4	0.354±0.011	0.107±0.002	0.193±0.004	0.511±0.054	Not Applicable	28707
	32	0.349±0.029	0.150±0.065	0.232±0.064	0.439±0.027	Not Applicable	53795
	128	0.395±0.043	0.249±0.110	0.304±0.095	0.517±0.068	Not Applicable	139811
NCDE	4	0.677±0.099	0.610±0.122	0.665±0.105	0.913±0.018	Not Applicable	21253
	32	0.759±0.047	0.690±0.065	0.756±0.052	0.907±0.016	Not Applicable	21253
	128	0.456±0.046	0.415±0.066	0.458±0.051	0.678±0.055	Not Applicable	21253
ANCDE	4	0.815±0.046	0.770±0.065	0.810±0.046	0.957±0.012	Not Applicable	92726
	32	0.774±0.033	0.727±0.060	0.770±0.033	0.925±0.021	Not Applicable	92726
	128	0.497±0.064	0.456±0.074	0.501±0.063	0.705±0.038	Not Applicable	22806
NRDE ₂	4	0.744±0.044	0.655±0.076	0.725±0.059	0.915±0.032	Not Applicable	64933
	32	0.779±0.029	0.713±0.044	0.774±0.027	0.934±0.011	Not Applicable	64933
	128	0.728±0.088	0.661±0.106	0.726±0.092	0.908±0.037	Not Applicable	64933
NRDE ₃	4	0.718±0.083	0.616±0.127	0.695±0.101	0.914±0.023	Not Applicable	297893
	32	0.810±0.043	0.787±0.051	0.814±0.044	0.911±0.020	Not Applicable	297893
	128	0.610±0.117	0.544±0.142	0.600±0.120	0.862±0.063	Not Applicable	297893
DE-NRDE ₂	4	0.436±0.048	0.230±0.073	0.303±0.066	0.538±0.045	Not Applicable	41331
	32	0.728±0.074	0.631±0.141	0.711±0.095	0.918±0.026	Not Applicable	41331
	128	0.769±0.068	0.723±0.078	0.770±0.070	0.939±0.016	Not Applicable	49304
DE-NRDE ₃	4	0.421±0.074	0.206±0.096	0.281±0.091	0.583±0.086	Not Applicable	179371
	32	0.626±0.047	0.528±0.038	0.585±0.054	0.878±0.036	Not Applicable	179371
	128	0.841±0.042	0.810±0.029	0.840±0.038	0.960±0.022	Not Applicable	241223
LORD _{1→2}	4	0.795±0.051	0.744±0.051	0.787±0.053	0.948±0.009	24299	38973
	32	0.841±0.053	0.841±0.058	0.843±0.051	0.957±0.016	24299	38973
	128	0.759±0.064	0.748±0.082	0.760±0.061	0.900±0.009	24299	34813
LORD _{1→3}	4	0.774±0.088	0.733±0.122	0.759±0.101	0.944±0.023	86907	34813
	32	0.862±0.053	0.855±0.058	0.861±0.054	0.963±0.021	86907	34813
	128	0.744±0.081	0.716±0.087	0.737±0.076	0.892±0.044	86907	38973
LORD _{2→3}	4	0.821±0.054	0.783±0.062	0.815±0.056	0.960±0.011	278679	132465
	32	0.841±0.021	0.793±0.053	0.835±0.027	0.963±0.008	278679	132465
	128	0.841±0.038	0.823±0.055	0.835±0.049	0.949±0.023	278679	128305

Table 11: CounterMovementJump

Method	P	Accuracy	Macro F1	Weighted F1	ROCAUC	#Params(D)	#Params(R)
ODE-RNN	64	0.474±0.023	0.453±0.027	0.455±0.026	0.589±0.018	Not Applicable	24737
	128	0.470±0.093	0.458±0.094	0.459±0.094	0.617±0.055	Not Applicable	213537
	512	0.449±0.032	0.436±0.037	0.436±0.039	0.593±0.031	Not Applicable	139425
NCDE	64	0.351±0.057	0.317±0.091	0.318±0.091	0.473±0.024	Not Applicable	58371
	128	0.404±0.064	0.350±0.050	0.352±0.050	0.520±0.007	Not Applicable	25475
	512	0.411±0.047	0.379±0.064	0.378±0.065	0.496±0.026	Not Applicable	46723
ANCDE	64	0.355±0.041	0.342±0.034	0.342±0.035	0.526±0.033	Not Applicable	135852
	128	0.467±0.060	0.457±0.065	0.457±0.065	0.604±0.031	Not Applicable	252332
	512	0.458±0.073	0.428±0.102	0.428±0.102	0.588±0.074	Not Applicable	285740
NRDE ₂	64	0.396±0.116	0.391±0.118	0.391±0.118	0.560±0.089	Not Applicable	107907
	128	0.396±0.076	0.379±0.079	0.379±0.078	0.513±0.052	Not Applicable	189059
	512	0.396±0.091	0.388±0.092	0.388±0.092	0.546±0.076	Not Applicable	50435
NRDE ₃	64	0.465±0.088	0.462±0.093	0.463±0.093	0.616±0.062	Not Applicable	529411
	128	0.409±0.084	0.399±0.081	0.400±0.081	0.573±0.070	Not Applicable	521859
	512	0.465±0.055	0.453±0.050	0.453±0.051	0.618±0.045	Not Applicable	2107395
DE-NRDE ₂	64	0.398±0.075	0.390±0.076	0.389±0.075	0.573±0.076	Not Applicable	51910
	128	0.384±0.058	0.334±0.071	0.334±0.071	0.567±0.054	Not Applicable	90886
	512	0.375±0.054	0.359±0.064	0.359±0.064	0.525±0.055	Not Applicable	39114
DE-NRDE ₃	64	0.409±0.072	0.373±0.073	0.373±0.074	0.568±0.068	Not Applicable	204300
	128	0.474±0.038	0.437±0.053	0.437±0.054	0.626±0.030	Not Applicable	279378
	512	0.425±0.069	0.396±0.076	0.398±0.076	0.571±0.059	Not Applicable	730892
LORD _{1→2}	64	0.589±0.038	0.580±0.041	0.580±0.041	0.717±0.023	3262	87191
	128	0.566±0.061	0.563±0.066	0.563±0.066	0.676±0.058	12158	51063
	512	0.501±0.080	0.495±0.082	0.495±0.082	0.638±0.053	7998	65399
LORD _{1→3}	64	0.555±0.041	0.551±0.042	0.550±0.042	0.688±0.038	7282	43127
	128	0.528±0.029	0.523±0.027	0.523±0.027	0.656±0.024	53746	137879
	512	0.508±0.033	0.499±0.028	0.499±0.028	0.637±0.020	8338	88439
LORD _{2→3}	64	0.396±0.049	0.383±0.052	0.383±0.052	0.540±0.061	77158	113265
	128	0.396±0.078	0.384±0.083	0.385±0.083	0.542±0.068	27110	146737
	512	0.400±0.044	0.374±0.022	0.375±0.022	0.537±0.047	31270	36369

D FULL EXPERIMENTAL RESULTS

In Tables 10 to 15, all experimental results are shown. #Params(D) and #Params(R) denote the number of parameters in the decoder part and in the rest parts except the decoder, respectively.

Table 12: SelfRegulationSCP2

Method	P	Accuracy	F1	ROCAUC	#Params(D)	#Params(R)
ODE-RNN	32	0.551±0.054	0.540±0.064	0.603±0.041	Not Applicable	57375
	64	0.579±0.012	0.462±0.051	0.564±0.019	Not Applicable	40991
	256	0.558±0.045	0.480±0.039	0.533±0.055	Not Applicable	139295
NCDE	32	0.586±0.071	0.471±0.124	0.577±0.130	Not Applicable	42241
	64	0.516±0.079	0.459±0.156	0.557±0.129	Not Applicable	214657
	256	0.544±0.058	0.537±0.087	0.578±0.086	Not Applicable	316161
ANCDE	32	0.604±0.064	0.552±0.048	0.646±0.041	Not Applicable	391698
	64	0.544±0.039	0.490±0.048	0.575±0.074	Not Applicable	134034
	256	0.488±0.052	0.427±0.067	0.461±0.073	Not Applicable	208914
NRDE ₂	32	0.519±0.110	0.513±0.058	0.572±0.092	Not Applicable	322689
	64	0.561±0.090	0.449±0.062	0.575±0.071	Not Applicable	622209
	256	0.516±0.110	0.498±0.071	0.564±0.096	Not Applicable	622209
NRDE ₃	32	0.537±0.052	0.560±0.050	0.561±0.049	Not Applicable	3402753
	64	0.558±0.059	0.504±0.118	0.586±0.107	Not Applicable	1710977
	256	0.498±0.066	0.483±0.074	0.543±0.079	Not Applicable	3438465
DE-NRDE ₂	32	0.589±0.095	0.525±0.130	0.596±0.072	Not Applicable	111051
	64	0.551±0.063	0.496±0.081	0.566±0.073	Not Applicable	196747
	256	0.530±0.078	0.501±0.078	0.538±0.088	Not Applicable	196747
DE-NRDE ₃	32	0.551±0.109	0.570±0.074	0.655±0.076	Not Applicable	1092158
	64	0.505±0.076	0.539±0.059	0.566±0.110	Not Applicable	542462
	256	0.512±0.100	0.547±0.031	0.591±0.069	Not Applicable	1137022
LORD _{1→2}	32	0.570±0.105	0.566±0.058	0.652±0.059	14572	24361
	64	0.582±0.119	0.613±0.057	0.681±0.071	76684	139433
	256	0.530±0.081	0.512±0.081	0.536±0.087	76684	74857
LORD _{1→3}	32	0.572±0.058	0.501±0.056	0.584±0.036	70132	138761
	64	0.618±0.099	0.591±0.109	0.659±0.094	71188	123241
	256	0.526±0.105	0.558±0.038	0.607±0.061	278452	161161
LORD _{2→3}	32	0.607±0.059	0.552±0.087	0.645±0.093	260580	216405
	64	0.607±0.095	0.555±0.072	0.619±0.060	999684	534037
	256	0.596±0.075	0.529±0.055	0.623±0.064	259524	254549

Table 13: BIDMC32HR

Method	P	R^2	Explained Variance	MSE	MAE	#Params(D)	#Params(R)
ODE-RNN	8	0.569±0.290	0.570±0.290	0.415±0.279	0.457±0.172	Not Applicable	3871
	128	0.924±0.011	0.925±0.011	0.073±0.011	0.167±0.009	Not Applicable	15391
	512	0.811±0.024	0.811±0.025	0.182±0.024	0.285±0.019	Not Applicable	52255
NCDE	8	0.388±0.042	0.388±0.042	0.590±0.041	0.552±0.023	Not Applicable	49921
	128	0.227±0.042	0.231±0.046	0.745±0.040	0.638±0.017	Not Applicable	49921
	512	0.191±0.041	0.192±0.041	0.779±0.039	0.654±0.018	Not Applicable	49921
ANCDE	8	0.437±0.031	0.440±0.031	0.542±0.030	0.527±0.019	Not Applicable	47194
	128	0.173±0.062	0.174±0.062	0.796±0.060	0.666±0.019	Not Applicable	47194
	512	0.264±0.011	0.270±0.012	0.709±0.011	0.628±0.016	Not Applicable	47194
NRDE ₂	8	0.630±0.044	0.631±0.044	0.356±0.042	0.452±0.030	Not Applicable	74689
	128	0.665±0.072	0.665±0.072	0.323±0.069	0.409±0.047	Not Applicable	74689
	512	0.642±0.071	0.643±0.071	0.344±0.069	0.419±0.054	Not Applicable	74689
NRDE ₃	8	0.650±0.082	0.650±0.082	0.337±0.079	0.430±0.054	Not Applicable	140737
	128	0.582±0.131	0.583±0.131	0.402±0.126	0.458±0.085	Not Applicable	140737
	512	0.395±0.131	0.396±0.131	0.582±0.126	0.535±0.039	Not Applicable	140737
DE-NRDE ₂	8	0.822±0.077	0.822±0.077	0.171±0.074	0.279±0.080	Not Applicable	63045
	128	0.758±0.051	0.759±0.052	0.233±0.049	0.332±0.045	Not Applicable	59589
	512	0.640±0.024	0.643±0.023	0.346±0.023	0.412±0.016	Not Applicable	58885
DE-NRDE ₃	8	0.885±0.049	0.885±0.049	0.111±0.048	0.222±0.050	Not Applicable	119050
	128	0.927±0.016	0.928±0.016	0.070±0.016	0.176±0.024	Not Applicable	102538
	512	0.810±0.085	0.810±0.086	0.183±0.082	0.299±0.080	Not Applicable	102538
LORD _{1→2}	8	0.979±0.006	0.979±0.006	0.020±0.005	0.084±0.014	10285	27277
	128	0.937±0.009	0.937±0.009	0.061±0.008	0.119±0.005	3277	34189
	512	0.441±0.039	0.443±0.041	0.538±0.038	0.479±0.033	3277	34189
LORD _{1→3}	8	0.982±0.005	0.982±0.005	0.018±0.005	0.079±0.008	12645	27277
	128	0.922±0.012	0.923±0.013	0.075±0.012	0.129±0.013	40997	65293
	512	0.450±0.031	0.452±0.029	0.530±0.030	0.474±0.007	4613	54925
LORD _{2→3}	8	0.978±0.006	0.979±0.006	0.021±0.006	0.078±0.009	15471	35563
	128	0.954±0.006	0.954±0.006	0.045±0.006	0.121±0.007	6095	51915
	512	0.848±0.043	0.849±0.043	0.146±0.041	0.216±0.028	15471	54283

Table 14: BIDMC32RR

Method	P	R^2	Explained Variance	MSE	MAE	#Params(D)	#Params(R)
ODE-RNN	8	0.536±0.195	0.540±0.193	0.447±0.188	0.494±0.124	Not Applicable	53791
	128	0.721±0.010	0.722±0.011	0.269±0.010	0.360±0.006	Not Applicable	122911
	512	0.651±0.018	0.652±0.017	0.337±0.018	0.413±0.016	Not Applicable	344095
NCDE	8	0.215±0.028	0.215±0.028	0.757±0.027	0.663±0.010	Not Applicable	86913
	128	0.337±0.053	0.339±0.053	0.639±0.051	0.595±0.015	Not Applicable	86913
	512	0.236±0.026	0.237±0.026	0.736±0.025	0.626±0.008	Not Applicable	86913
ANCDE	8	0.298±0.062	0.302±0.064	0.677±0.060	0.625±0.033	Not Applicable	47194
	128	0.386±0.097	0.387±0.098	0.592±0.094	0.576±0.036	Not Applicable	47194
	512	0.270±0.028	0.271±0.028	0.704±0.027	0.619±0.010	Not Applicable	55514
NRDE ₂	8	0.274±0.037	0.274±0.037	0.700±0.035	0.637±0.019	Not Applicable	123969
	128	0.521±0.082	0.521±0.082	0.462±0.079	0.500±0.035	Not Applicable	123969
	512	0.498±0.162	0.498±0.162	0.484±0.156	0.512±0.075	Not Applicable	123969
NRDE ₃	8	0.337±0.035	0.338±0.035	0.639±0.034	0.600±0.019	Not Applicable	222785
	128	0.646±0.138	0.647±0.138	0.341±0.133	0.403±0.087	Not Applicable	222785
	512	0.424±0.130	0.424±0.130	0.556±0.126	0.537±0.071	Not Applicable	222785
DE-NRDE ₂	8	0.644±0.013	0.647±0.012	0.343±0.013	0.388±0.017	Not Applicable	88196
	128	0.584±0.061	0.586±0.060	0.401±0.059	0.440±0.036	Not Applicable	100677
	512	0.552±0.063	0.554±0.061	0.432±0.061	0.474±0.033	Not Applicable	99973
DE-NRDE ₃	8	0.699±0.055	0.699±0.055	0.290±0.053	0.351±0.041	Not Applicable	139144
	128	0.703±0.017	0.703±0.017	0.287±0.016	0.352±0.015	Not Applicable	164106
	512	0.574±0.053	0.575±0.054	0.411±0.051	0.454±0.025	Not Applicable	162570
LORD _{1→2}	8	0.808±0.021	0.809±0.022	0.185±0.020	0.272±0.011	10285	27277
	128	0.662±0.007	0.664±0.007	0.326±0.006	0.386±0.012	10285	27277
	512	0.448±0.044	0.450±0.044	0.532±0.042	0.522±0.012	10285	39757
LORD _{1→3}	8	0.798±0.017	0.799±0.017	0.195±0.016	0.277±0.014	12645	27277
	128	0.671±0.016	0.672±0.015	0.318±0.015	0.376±0.012	12645	44973
	512	0.451±0.026	0.453±0.023	0.530±0.025	0.520±0.012	12645	44973
LORD _{2→3}	8	0.800±0.007	0.801±0.007	0.192±0.007	0.281±0.008	15471	35563
	128	0.744±0.011	0.744±0.011	0.247±0.010	0.315±0.010	15471	136459
	512	0.662±0.015	0.664±0.014	0.326±0.014	0.386±0.011	46511	103531

Table 15: BIDMC32SpO2

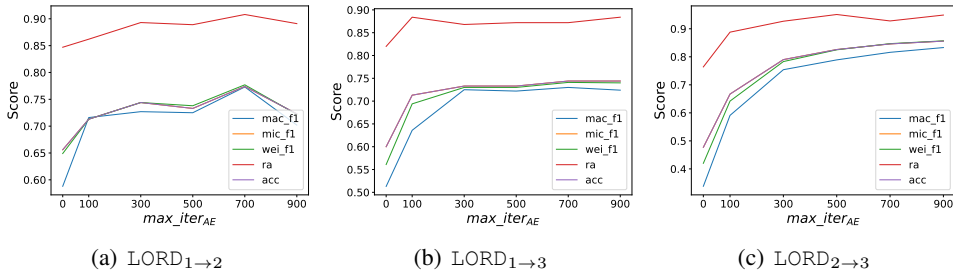
Method	P	R^2	Explained Variance	MSE	MAE	#Params(D)	#Params(R)
ODE-RNN	8	0.551±0.108	0.552±0.108	0.464±0.112	0.487±0.082	Not Applicable	3871
	128	0.899±0.025	0.901±0.023	0.104±0.026	0.225±0.035	Not Applicable	15391
	512	0.749±0.024	0.749±0.024	0.259±0.025	0.365±0.021	Not Applicable	52255
NCDE	8	0.240±0.071	0.245±0.067	0.785±0.073	0.686±0.034	Not Applicable	86913
	128	0.215±0.074	0.217±0.072	0.811±0.077	0.694±0.035	Not Applicable	86913
	512	0.328±0.045	0.332±0.045	0.694±0.046	0.639±0.037	Not Applicable	86913
ANCDE	8	0.311±0.034	0.313±0.035	0.712±0.035	0.662±0.014	Not Applicable	47194
	128	0.327±0.049	0.327±0.049	0.696±0.050	0.631±0.017	Not Applicable	47194
	512	0.372±0.033	0.374±0.034	0.648±0.034	0.592±0.013	Not Applicable	47194
NRDE ₂	8	0.218±0.078	0.219±0.078	0.807±0.080	0.694±0.036	Not Applicable	123969
	128	0.470±0.100	0.471±0.100	0.547±0.103	0.559±0.048	Not Applicable	123969
	512	0.607±0.180	0.607±0.180	0.406±0.186	0.455±0.123	Not Applicable	123969
NRDE ₃	8	0.131±0.091	0.134±0.090	0.898±0.094	0.720±0.027	Not Applicable	222785
	128	0.681±0.147	0.681±0.147	0.330±0.151	0.410±0.126	Not Applicable	222785
	512	0.596±0.181	0.596±0.181	0.417±0.187	0.463±0.139	Not Applicable	222785
DE-NRDE ₂	8	0.854±0.013	0.854±0.013	0.151±0.013	0.252±0.015	Not Applicable	88196
	128	0.740±0.047	0.740±0.048	0.269±0.049	0.313±0.039	Not Applicable	99973
	512	0.586±0.042	0.586±0.042	0.428±0.043	0.453±0.033	Not Applicable	99973
DE-NRDE ₃	8	0.903±0.079	0.903±0.079	0.100±0.082	0.192±0.090	Not Applicable	139144
	128	0.926±0.026	0.927±0.026	0.076±0.027	0.164±0.024	Not Applicable	162570
	512	0.759±0.067	0.761±0.067	0.249±0.069	0.357±0.061	Not Applicable	162570
LORD _{1→2}	8	0.975±0.003	0.976±0.002	0.025±0.003	0.096±0.009	10285	27277
	128	0.909±0.009	0.910±0.009	0.094±0.009	0.172±0.013	3277	34189
	512	0.583±0.047	0.583±0.047	0.431±0.048	0.435±0.024	10285	61549
LORD _{1→3}	8	0.981±0.005	0.981±0.004	0.020±0.005	0.086±0.006	12645	27277
	128	0.889±0.025	0.889±0.025	0.115±0.026	0.186±0.029	12645	27277
	512	0.521±0.045	0.522±0.044	0.495±0.046	0.459±0.024	4613	38349
LORD _{2→3}	8	0.981±0.005	0.981±0.005	0.019±0.005	0.088±0.007	15471	35563
	128	0.940±0.007	0.940±0.007	0.062±0.007	0.145±0.004	15471	56395
	512	0.829±0.027	0.830±0.027	0.177±0.028	0.236±0.016	46511	69323

Table 16: Sensitivity of max_iter_{AE} in EigenWorms ($P = 128$)

Method	max_iter_{AE}	Accuracy	Macro F1	Weighted F1	ROCAUC
LORD ₁ → ₂	0	0.656±0.094	0.588±0.107	0.649±0.100	0.847±0.056
	100	0.713±0.042	0.716±0.058	0.713±0.046	0.862±0.023
	300	0.744±0.048	0.727±0.059	0.744±0.051	0.893±0.029
	500	0.733±0.105	0.725±0.104	0.738±0.111	0.889±0.035
	700	0.774±0.049	0.773±0.070	0.777±0.056	0.908±0.026
	900	0.723±0.091	0.702±0.092	0.722±0.083	0.891±0.054
LORD ₁ → ₃	0	0.600±0.140	0.513±0.215	0.561±0.188	0.820±0.068
	100	0.713±0.056	0.636±0.139	0.694±0.085	0.884±0.030
	300	0.733±0.069	0.725±0.053	0.730±0.063	0.868±0.036
	500	0.733±0.039	0.722±0.054	0.730±0.046	0.872±0.035
	700	0.744±0.031	0.730±0.043	0.741±0.034	0.872±0.021
	900	0.744±0.048	0.724±0.040	0.740±0.053	0.884±0.015
LORD ₂ → ₃	0	0.477±0.059	0.338±0.105	0.420±0.078	0.764±0.051
	100	0.667±0.091	0.591±0.127	0.642±0.106	0.888±0.044
	300	0.790±0.042	0.754±0.060	0.783±0.050	0.927±0.017
	500	0.826±0.071	0.789±0.113	0.825±0.072	0.951±0.029
	700	0.846±0.101	0.816±0.126	0.847±0.103	0.928±0.046
	900	0.856±0.067	0.833±0.087	0.857±0.067	0.949±0.027

E SENSITIVITY EXPERIMENTS

Fig. 6 and Table 16 show that in general, the performance of LORD is improved as max_iter_{AE} gets larger in EigenWorms ($P = 128$). Our encoder-decoder structure can successfully integrate the lower-depth log-signature and the higher-depth log-signature information into the embedding vector e , and the well-integrated information helps the model perform better. In general, the lower-depth and the higher-depth log-signature information are blended better as the encoder-decoder structure is more trained.

Figure 6: Sensitivity to max_iter_{AE}

F TRAIN LOSS

Fig. 7 visualizes several training cases for our method and the original NRDE design. In general, our method shows much better stability across the entire training period.

G END-TO-END TRAINING

LORD has two distinguished characteristics in its training process. First, LORD uses a two-phase training strategy, a pre-training and a main training processes. Second, the training process of LORD is not end-to-end. In other words, the decoder is not used and the encoder is fixed in the main training phase. In this section, we test with various end-to-end-training settings for LORD.

There are three possible configurations for the end-to-end-training. The first configuration is training the encoder (rather than fixing it) with L_{TASK} in the main training phase, which is denoted as FineTuning. The second one is Co-Train where both L_{AE} and L_{TASK} are used for training the encoder, the decoder and the main NRDE — recall that in FineTuning, we use only L_{TASK}

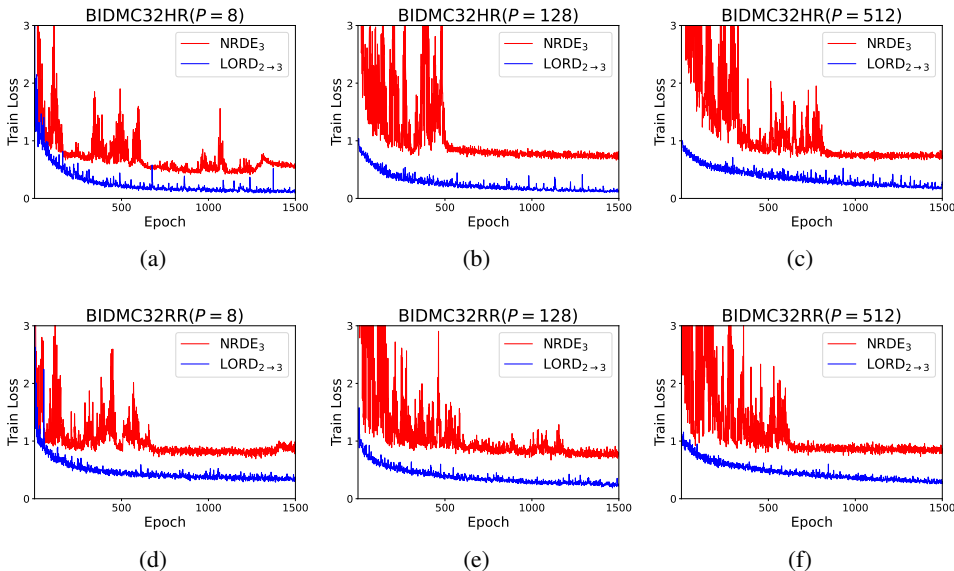


Figure 7: Train loss of $NRDE_3$ and $LORD_{2 \rightarrow 3}$

Table 17: Comparison between LORD and its various end-to-end training variations in EigenWorms ($P = 128$)

Method	Accuracy	Macro F1	Weighted F1	ROCAUC	
LORD	0.759±0.064	0.748±0.082	0.760±0.061	0.900±0.009	
$LORD_{1 \rightarrow 2}$	FineTuning	0.744±0.075	0.726±0.086	0.740±0.077	0.882±0.042
	Co-Train	0.718±0.021	0.686±0.025	0.715±0.014	0.865±0.030
	Co-Train(w.o. pre)	0.679±0.033	0.650±0.031	0.669±0.029	0.832±0.013
$LORD_{1 \rightarrow 3}$	LORD	0.744±0.081	0.716±0.087	0.737±0.076	0.892±0.044
	FineTuning	0.692±0.055	0.649±0.049	0.680±0.069	0.865±0.018
	Co-Train	0.744±0.036	0.723±0.059	0.741±0.037	0.868±0.022
	Co-Train(w.o. pre)	0.692±0.069	0.674±0.083	0.694±0.064	0.839±0.066
$LORD_{2 \rightarrow 3}$	LORD	0.841±0.038	0.823±0.055	0.835±0.049	0.949±0.023
	FineTuning	0.731±0.061	0.687±0.075	0.714±0.062	0.919±0.005
	Co-Train	0.808±0.061	0.772±0.074	0.803±0.071	0.948±0.021
	Co-Train(w.o. pre)	0.583±0.112	0.499±0.145	0.557±0.117	0.804±0.065

to train the encoder. The last method is Co-Train (w.o. pre) which is the same as Co-Train without any pre-training process. The same hyperparameters are used for all end-to-end models.

We experiment with EigenWorms ($P = 128$). Table 16 shows the results. Among the three end-to-end models, Co-Train shows the best performance. Co-Train (w.o. pre) has the worst performance in general. These results prove that the pre-training makes the main training easier.

Table 18: The best hyperparameter in ODE-RNN

Data	P	Hidden Path Size
Character-Trajectory	1	128
	4	128
	16	256
	32	64
LiveFuel-MoistureContent	1	128
	4	64
	16	64
	32	128

Table 19: The best hyperparameter in NCDE and NRDE

Data	P	Hidden Path Size			CDE Function's Hidden Size			#Hidden Layers		
		$D = 1$	2	3	1	2	3	1	2	3
Character-Trajectory	1	64	-	-	256	-	-	3	-	-
	4	128	256	64	256	256	128	3	3	2
	16	256	256	128	64	64	256	2	3	2
	32	256	128	128	64	64	128	2	3	2
LiveFuel-MoistureContent	1	64	-	-	64	-	-	3	-	-
	4	64	128	128	128	256	64	3	3	2
	16	64	256	64	64	256	256	2	3	2
	32	256	256	64	256	128	64	3	3	2

Table 20: The best hyperparameter in ANCDE

Data	P	Hidden Path Size	#Hidden Layers	Attention Channel Size
Character-Trajectory	1	256	3	256
	4	256	2	64
	16	256	3	64
LiveFuel-MoistureContent	32	256	2	64
	1	128	3	64
	4	128	3	128
MoistureContent	16	128	2	64
	32	256	3	64

Table 21: The best hyperparameter in DE-NRDE

Data	P	Compression Ratio		#Hidden Layers		Hidden Size	
		$D = 2$	3	2	3	2	3
Character-Trajectory	4	0.7	0.3	1	1	64	128
	16	0.5	0.5	1	1	128	64
	32	0.7	0.5	1	2	128	128
LiveFuel-MoistureContent	4	0.7	0.7	2	2	64	128
	16	0.3	0.3	2	1	64	64
	32	0.7	0.5	2	2	128	64

Table 22: The best hyperparameter in LORD

Method	Data	P	N_f	N_g	N_o	h_f	h_g	h_o	c_{AE}	c_{TASK}	c_e	max_{iter} AE TASK	
LORD _{1→2}	Character-Trajectory	4	3	3	3	64	256	64	1×10^{-6}	1×10^{-6}	0	1000	400
		16	3	3	3	64	128	64	1×10^{-6}	1×10^{-6}	0	1000	400
		32	3	3	3	128	256	128	1×10^{-6}	1×10^{-6}	0	1000	400
	LiveFuel-MoistureContent	4	3	3	3	128	128	128	1×10^{-6}	1×10^{-6}	0	2000	400
		16	3	3	3	256	256	256	1×10^{-6}	1×10^{-6}	0	2000	400
		32	3	3	3	256	256	256	1×10^{-6}	1×10^{-6}	0	1500	400
LORD _{1→3}	Character-Trajectory	4	3	3	3	128	128	128	1×10^{-6}	1×10^{-6}	0	1000	400
		16	3	3	3	128	128	128	1×10^{-6}	1×10^{-6}	0	1000	400
		32	3	3	3	128	64	128	1×10^{-6}	1×10^{-6}	0	1000	400
	LiveFuel-MoistureContent	4	3	3	3	256	256	256	1×10^{-6}	1×10^{-6}	0	2000	400
		16	3	3	3	64	64	64	1×10^{-6}	1×10^{-6}	0	2000	400
		32	3	3	3	128	64	128	1×10^{-6}	1×10^{-6}	0	1500	400
LORD _{2→3}	Character-Trajectory	4	3	3	3	128	256	128	1×10^{-6}	1×10^{-6}	0	1000	400
		16	3	3	3	256	256	256	1×10^{-6}	1×10^{-6}	0	1000	400
		32	3	3	3	128	256	128	1×10^{-6}	1×10^{-6}	0	1000	400
	LiveFuel-MoistureContent	4	3	3	3	256	64	256	1×10^{-6}	1×10^{-6}	0	2000	400
		16	3	3	3	128	256	128	1×10^{-6}	1×10^{-6}	0	2000	400
		32	3	3	3	64	256	64	1×10^{-6}	1×10^{-6}	0	1500	400

H ADDITIONAL EXPERIMENTS WITH SHORT TIME-SERIES

In this section, we experiment with short time-series datasets. We use CharacterTrajectory and LiveFuelMoistureContent from (Bagnall A.). The object of CharacterTrajectory is to classify 20 characters using the trajectory information of writing on a tablet. Its length is 182. LiveFuelMoistureContent consists of daily reflectance data at 7 spectral bands for predicting moisture rate in vegetation. Its length is 365. In Tables 18 to 22, we summarize hyperparameters. Because of the short time-series lengths, we test $P = 1$ for all except NRDE-based models.

In Table 23, NRDE achieves the best scores among baseline models and LORD achieves the best scores among all methods. In Table 24, DE-NRDE₂ is the best. Except DE-NRDE₂, ODE-RNN is the best. However, LORD also has comparable scores. From these results, NRDE and NRDE-based models are empirically useful for short-time series as well.

Table 23: CharacterTrajectory

Method	P	Accuracy	Macro F1	Weighted F1	ROCAUC	#Params(D)	#Params(R)
ODE-RNN	1	0.716±0.036	0.697±0.041	0.712±0.038	0.969±0.007	Not Applicable	27570
	4	0.950±0.012	0.947±0.013	0.950±0.012	0.998±0.001	Not Applicable	29106
	16	0.968±0.004	0.967±0.005	0.968±0.004	0.999±0.000*	Not Applicable	103218
	32	0.962±0.009	0.959±0.010	0.962±0.009	0.997±0.001	Not Applicable	17650
NCDE	1	0.954±0.004	0.952±0.004	0.954±0.004	0.998±0.000	Not Applicable	149844
	4	0.951±0.005	0.948±0.005	0.951±0.005	0.998±0.000	Not Applicable	233620
	16	0.905±0.020	0.901±0.020	0.905±0.020	0.994±0.002	Not Applicable	93588
	32	0.829±0.012	0.818±0.013	0.828±0.012	0.983±0.002	Not Applicable	93588
ANCDE	1	0.959±0.007	0.958±0.007	0.959±0.007	0.998±0.000	Not Applicable	669757
	4	0.952±0.008	0.950±0.008	0.952±0.008	0.998±0.000	Not Applicable	286845
	16	0.897±0.009	0.893±0.011	0.896±0.010	0.994±0.001	Not Applicable	538173
	32	0.777±0.020	0.762±0.020	0.774±0.021	0.981±0.001	Not Applicable	103293
NRDE ₂	4	0.970±0.004	0.968±0.005	0.970±0.004	0.999±0.000*	Not Applicable	795924
	16	0.951±0.008	0.949±0.009	0.951±0.008	0.998±0.001	Not Applicable	193428
	32	0.950±0.007	0.948±0.008	0.950±0.007	0.998±0.000	Not Applicable	98836
NRDE ₃	4	0.966±0.006	0.965±0.006	0.966±0.006	0.999±0.000*	Not Applicable	274132
	16	0.960±0.006	0.960±0.006	0.961±0.006	0.999±0.000*	Not Applicable	531604
	32	0.961±0.002	0.959±0.002	0.961±0.002	0.999±0.000*	Not Applicable	1088916
DE-NRDE ₂	4	0.898±0.077	0.890±0.084	0.897±0.078	0.994±0.007	Not Applicable	599707
	16	0.907±0.013	0.900±0.012	0.906±0.012	0.996±0.002	Not Applicable	112281
	32	0.897±0.018	0.890±0.018	0.896±0.017	0.995±0.001	Not Applicable	76187
DE-NRDE ₃	4	0.933±0.031	0.926±0.035	0.932±0.032	0.997±0.001	Not Applicable	105885
	16	0.947±0.014	0.943±0.015	0.947±0.014	0.998±0.000	Not Applicable	286883
	32	0.913±0.013	0.907±0.014	0.912±0.013	0.996±0.001	Not Applicable	617891
LORD _{1→2}	4	0.977±0.002*	0.976±0.003*	0.977±0.002*	0.999±0.000*	12158	235880
	16	0.955±0.010	0.953±0.010	0.955±0.010	0.998±0.001	12158	96232
	32	0.829±0.069	0.817±0.077	0.826±0.074	0.985±0.011	40126	261928
LORD _{1→3}	4	0.976±0.005	0.975±0.006	0.976±0.005	0.999±0.000*	53746	98568
	16	0.959±0.006	0.957±0.006	0.959±0.006	0.998±0.001	53746	98568
	32	0.810±0.069	0.796±0.074	0.808±0.071	0.983±0.013	53746	63560
LORD _{2→3}	4	0.971±0.008	0.969±0.009	0.971±0.008	0.999±0.000*	77158	372418
	16	0.971±0.003	0.969±0.003	0.971±0.003	0.999±0.000*	218086	391650
	32	0.964±0.008	0.963±0.008	0.964±0.008	0.999±0.000*	77158	372418

Table 24: LiveFuelMoistureContent

Method	P	R^2	Explained Variance	MSE	MAE	#Params(D)	#Params(R)
ODE-RNN	1	0.026±0.005	0.026±0.005	1.064±0.005	0.775±0.001	Not Applicable	25631
	4	0.029±0.003	0.029±0.003	1.062±0.003	0.774±0.002	Not Applicable	10271
	16	0.032±0.003	0.033±0.003	1.058±0.004	0.775±0.004	Not Applicable	16415
	32	0.031±0.004	0.031±0.004	1.059±0.004	0.774±0.003	Not Applicable	57375
NCDE	1	-0.009±0.037	-0.008±0.037	1.102±0.040	0.787±0.010	Not Applicable	42241
	4	-0.004±0.020	-0.003±0.020	1.098±0.022	0.785±0.007	Not Applicable	91521
	16	-0.043±0.031	-0.043±0.031	1.140±0.034	0.794±0.011	Not Applicable	42241
	32	0.009±0.029	0.009±0.029	1.083±0.032	0.779±0.005	Not Applicable	660481
ANCDE	1	-0.025±0.078	-0.024±0.079	1.120±0.086	0.785±0.009	Not Applicable	101714
	4	0.014±0.007	0.015±0.007	1.077±0.007	0.781±0.003	Not Applicable	241938
	16	0.003±0.030	0.004±0.030	1.089±0.033	0.781±0.010	Not Applicable	93394
	32	0.006±0.017	0.006±0.017	1.087±0.019	0.784±0.009	Not Applicable	177746
NRDE ₂	4	-0.010±0.043	-0.009±0.043	1.103±0.047	0.785±0.004	Not Applicable	1284353
	16	-0.373±0.274	-0.373±0.274	1.501±0.299	0.824±0.020	Not Applicable	2502657
	32	-0.151±0.166	-0.151±0.166	1.258±0.182	0.816±0.023	Not Applicable	1240833
NRDE ₃	4	-0.480±0.311	-0.480±0.311	1.618±0.340	0.830±0.012	Not Applicable	1710977
	16	-1.308±2.265	-1.307±2.264	2.522±2.475	0.863±0.089	Not Applicable	3438465
	32	-2.183±4.622	-2.182±4.621	3.478±5.051	0.896±0.174	Not Applicable	857601
DE-NRDE ₂	4	0.040±0.007	0.040±0.007	1.049±0.007	0.770±0.005	Not Applicable	930650
	16	0.042±0.006	0.042±0.006	1.047±0.007	0.768±0.005	Not Applicable	799243
	32	0.043±0.005*	0.043±0.005*	1.046±0.006*	0.767±0.006*	Not Applicable	902042
DE-NRDE ₃	4	-0.778±1.599	-0.776±1.599	1.943±1.747	0.796±0.039	Not Applicable	1256207
	16	-0.037±0.046	-0.036±0.046	1.133±0.051	0.790±0.010	Not Applicable	1103486
	32	-0.657±0.831	-0.651±0.822	1.810±0.908	0.829±0.045	Not Applicable	457191
LORD _{1→2}	4	0.017±0.015	0.018±0.014	1.074±0.016	0.784±0.011	76684	120937
	16	0.019±0.007	0.020±0.008	1.072±0.008	0.781±0.007	216844	441481
	32	0.013±0.007	0.014±0.007	1.078±0.007	0.784±0.002	216844	441481
LORD _{1→3}	4	0.018±0.010	0.018±0.011	1.074±0.011	0.782±0.006	612148	441481
	16	0.002±0.009	0.003±0.009	1.091±0.010	0.790±0.003	136180	70153
	32	0.005±0.011	0.005±0.010	1.087±0.012	0.788±0.007	278452	99529
LORD _{2→3}	4	-0.025±0.037	-0.025±0.038	1.120±0.041	0.793±0.004	2081028	648629
	16	-0.015±0.027	-0.014±0.027	1.109±0.030	0.793±0.004	1016196	957557
	32	0.008±0.002	0.008±0.002	1.085±0.003	0.788±0.002	508356	540181